Analytical design of conformally invisible cloaks for arbitrarily shaped objects

Wei Xiang Jiang, Jessie Yao Chin, Zhuo Li, Qiang Cheng, Ruopeng Liu, and Tie Jun Cui*
State Key Laboratory of Millimeter Waves, Department of Radio Engineering, Southeast University, Nanjing 210096, China
(Received 27 January 2008; revised manuscript received 7 April 2008; published 25 June 2008)

To design conformally invisible cloaks for arbitrarily shaped objects, we use the nonuniform rational *B*-spline (NURBS) to represent the geometrical modeling of the arbitrary object. Based on the method of optical transformation, analytical formulas of the permittivity and permeability tensors are proposed for arbitrarily shaped invisible cloaks. Such formulas can be easily implemented in the design of arbitrary cloaks. Full-wave simulations are given for heart-shaped invisible cloaks and perfectly electrical conducting (PEC) objects, in which we observe that the power-flow lines of incoming electromagnetic waves will be bent smoothly in the cloaks and will return to their original propagation directions after propagating around the object. We also show that the scattered field from the PEC object coated with the invisible cloak is much smaller than that from the PEC core. The application of NURBS in the design of arbitrary cloaks shows transformation optics to be a very general tool to interface with commercial softwares like 3D STUDIOMAX and MAYA.

DOI: 10.1103/PhysRevE.77.066607 PACS number(s): 41.20.Jb, 42.25.Gy, 42.79.Dj

I. INTRODUCTION

Since Pendry *et al.* and Leonhardt proposed the interesting idea to design an invisible cloak using the coordinate transformation method [1,2], more and more attention has been focused on spherical and circularly cylindrical cloaks [3–15]. The first practical cloak with simplified medium parameters was verified in the microwave frequency range [3]. Inspired by such an idea, other applications such as the rotation of electromagnetic (EM) waves [16], reflectionless complex media [17], and EM-wave concentrators [18] have been proposed. Invisibility with respect to solutions of the Helmholtz and Maxwell equations has also been proposed for the construction of several cloaking devices at all frequencies [19].

However, most works in the literature [3–15] on invisible cloaks have focused attention on circular and spherical shapes, which are relatively easier to design and analyze. Recently, based on the metric invariance of Maxwell's equations, constitutive tensors of EM masking as arbitrarily shaped convex conducting objects has been derived [20]. Such a masking can be regarded as a partial cloaking layer. Only when the ratio between the maximum and minimum radii of the object approaches 1—i.e., the object is a sphere—could the masking be equivalent to an invisible cloak [20]. Although a square-shaped invisible cloak has been reported more recently [21], design formulas for arbitrarily shaped cloaks are still unavailable.

In this paper, we introduce the nonuniform rational *B*-spline (NURBS) [22] to represent the geometric modeling of any objects, from which the design of conformally invisible cloaks is presented based on the coordinate transformation. An arbitrarily shaped object can be divided into several parts with each part described by NURBS. Then the conformal cloak will also be divided into several parts. We will construct the coordinate transformation in each part from free space to a vaulted region. Analytical formulas of the permittivity and permeability tensors are proposed for the arbitrarily shaped invisible cloaks. As examples, the simulation results of two different heart-shaped cloaks are presented to validate the design.

II. CONFORMALLY INVISIBLE CLOAKS FOR ARBITRARILY SHAPED OBJECTS

Implicit functions and parametric equations are the two most common methods to represent arbitrary curves in geometrical modeling. As one of the parametric-curve representations, NURBS is a very popular scheme, from which it is usually possible to split an arbitrary curve into a sequence of rational Bézier curves approximately. The rational Bézier curves of second order can represent all conic sections—circles, ellipses, parabolas, and hyperbolas—and they are easier to handle. Hence we use piecewise rational Bézier curves to represent the geometric models of arbitrary objects approximately.

A second-order curve consists of three control vertices and three weights, as illustrated in Fig. 1. Furthermore, the Bézier curve may be either a rational Bézier curve or a polynomial Bézier curve since a rational Bézier curve is equivalent to a polynomial Bézier curve when the control weights are the same.

In this paper, we will investigate two-dimensional (2D) arbitrarily cylindrical cloaks since 2D cloaks are more fea-

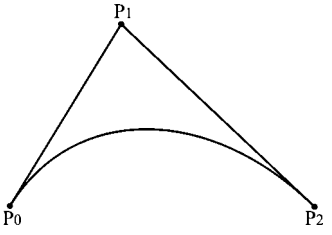

FIG. 1. The second-order Bézier curve with three control points P_0, P_1, and P_2.

*tjcui@seu.edu.cn

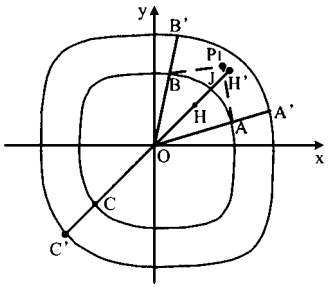

FIG. 2. The cross sections of an arbitrarily shaped object and the conformal cloak in the Cartesian coordinate system, in which H is an arbitrary point in the original space and H' is the corresponding point in the transformed space.

sible to realize [3]. We first consider a section of an arbitrary object, which is covered by a conformal cloaking shell, as shown in Fig. 2. The boundary of the section can be represented by a Bézier curve accurately, whose control points are $A(a_0,b_0)$, $P_1(a_1,b_1)$, and $B(a_2,b_2)$ and control weights are w_0, w_1, and w_2, respectively. The parametric equations of the curve can be written as

$$x(u) = \frac{w_0 a_0 (1-u)^2 + 2w_1 a_1 (1-u)u + w_2 a_2 u^2}{w_0 (1-u)^2 + 2w_1 (1-u)u + w_2 u^2}, \tag{1}$$

$$y(u) = \frac{w_0 b_0 (1-u)^2 + 2w_1 b_1 (1-u)u + w_2 b_2 u^2}{w_0 (1-u)^2 + 2w_1 (1-u)u + w_2 u^2}, \tag{2}$$

where u is a positive parameter $(0 \le u \le 1)$.

Now we want to compress the space $A'OB'$ into the shell space $A'ABB'$ using a coordinate transformation. Choose an arbitrary point $H(x,y)$ in the original coordinate system; its corresponding point is $H'(x',y')$ in the transformed system, as shown in Fig. 2. We denote the distance OH as $r = \sqrt{x^2+y^2}$ and OH' as $r' = \sqrt{x'^2+y'^2}$. Then the coordinate transformation equation from the original space to the new space is expressed as

$$r' = \frac{|OA'| - |OA|}{|OA'|} r + R_1, \tag{3}$$

in which R_1 is the distance of OJ and J is the intersection point of OH' and the inner Bézier curve.

In order to obtain a conformally invisible cloak, we employ a conformal transformation

$$\frac{|OC'| - |OC|}{|OC'|} = \frac{|OA'| - |OA|}{|OA'|},$$

which holds for any point C' on the outer boundary. Here, C is the joint point of OC' and the inner boundary. We denote the slopes of OH, OA, and OB as t, t_0, and t_2. Then the slopes of OH' and OJ are also t. As a consequence, we easily have

$$\frac{w_0 b_0 (1-u)^2 + 2w_1 b_1 (1-u)u + w_2 b_2 u^2}{w_0 a_0 (1-u)^2 + 2w_1 a_1 (1-u)u + w_2 a_2 u^2} = t, \tag{4}$$

which is also expressed as

$$\begin{aligned}&[(w_0 a_0 - 2w_1 a_1 + w_2 a_2)t - (w_0 a_0 - 2w_1 a_1 + w_2 a_2)]u^2 \\ &+ [(-2w_0 a_0 + 2w_1 a_1)t + 2w_0 b_0 - 2w_1 b_1]u \\ &+ w_0 a_0 t - w_0 b_0 = 0.\end{aligned}$$

Let $L = (w_0 a_0 - 2w_1 a_1 + w_2 a_2)t - (w_0 a_0 - 2w_1 a_1 + w_2 a_2)$, $M = (-2w_0 a_0 + 2w_1 a_1)t + 2w_0 b_0 - 2w_1 b_1$, and $N = w_0 a_0 t - w_0 b_0$; the solution is then obtained as

$$u = \frac{-M \pm \sqrt{M^2 - 4LN}}{2L}, \tag{5}$$

in which the "+" or "−" sign is determined by the following two conditions: (a) $u=0$, if $t=t_0$; (b) $u=1$, if $t=t_2$.

Hence the solution to Eq. (4) is determined and we can get the coordinates at the point J (x_J, y_J) from Eqs. (1) and (2) and, furthermore, the length of OJ as $R_1 = R(x,y)$ or $R_1 = R'(x',y')$. We define the operators $\mathbf{A} = R(x,y)/r$ and $\mathbf{A}' = R'(x',y')/r'$. Due to the transformation invariance, the unit vectors in the original and transformed spaces must be equal [4]: $x'/r' = x/r$ and $y'/r' = y/r$. Let

$$k = \frac{|OA'| - |OA|}{|OA'|};$$

then, the coordinate transformation formulas can be expressed as

$$x' = (k + \mathbf{A})x, \tag{6}$$

$$y' = (k + \mathbf{A})y, \tag{7}$$

$$z' = z. \tag{8}$$

With the above equations, we can easily obtain the Jacobian transformation matrix [4] as

$$\bar{\Lambda} = \begin{pmatrix} \frac{\partial x'}{\partial x} & \frac{\partial x'}{\partial y} & 0 \\ \frac{\partial y'}{\partial x} & \frac{\partial y'}{\partial y} & 0 \\ 0 & 0 & 1 \end{pmatrix} \tag{9}$$

$$= \begin{pmatrix} k + \mathbf{A} + x\mathbf{A}_x & x\mathbf{A}_y & 0 \\ y\mathbf{A}_x & k + \mathbf{A} + y\mathbf{A}_y & 0 \\ 0 & 0 & 1 \end{pmatrix}, \tag{10}$$

in which $\mathbf{A}_x$ and $\mathbf{A}_y$ represent the derivatives of $\mathbf{A}$ with respect to x and y, respectively. The determinant of the Jacobian matrix has a closed-form expression

$$\det(\bar{\Lambda}) = (k + \mathbf{A})^2 + (k + \mathbf{A})(x\mathbf{A}_x + y\mathbf{A}_y). \tag{11}$$

By metric invariance of Maxwell's equations, we then obtain the constitutive parameter tensors of the medium in the transformed space as [4]

$$\bar{\varepsilon}' = \frac{\bar{\Lambda} \cdot \bar{\varepsilon} \cdot \bar{\Lambda}^T}{\det(\bar{\Lambda})}, \tag{12}$$

$$\overline{\mu'} = \frac{\bar{\Lambda} \cdot \bar{\mu} \cdot \bar{\Lambda}^T}{\det(\bar{\Lambda})}, \tag{13}$$

in which an $\exp(-i\omega t)$ time dependence has been assumed. In our study, we assume the original space be free space: $\bar{\varepsilon} = \bar{\mathbf{I}}\varepsilon_0$ and $\bar{\mu} = \bar{\mathbf{I}}\mu_0$. Hence the relative permittivity and permeability tensors in the cloaking region can be expressed as

$$\overline{\varepsilon_r'} = \overline{\mu_r'} = \begin{pmatrix} \varepsilon_{xx} & \varepsilon_{xy} & 0 \\ \varepsilon_{yx} & \varepsilon_{yy} & 0 \\ 0 & 0 & \varepsilon_{zz} \end{pmatrix}, \tag{14}$$

in which

$$\varepsilon_{xx} = \frac{(k+\mathbf{A})^2 + 2(k+\mathbf{A})x\mathbf{A}_x + x^2(\mathbf{A}_x^2 + \mathbf{A}_y^2)}{\det(\bar{\Lambda})}, \tag{15}$$

$$\varepsilon_{xy} = \frac{(k+\mathbf{A})(y\mathbf{A}_x + x\mathbf{A}_y) + xy(\mathbf{A}_y^2 + \mathbf{A}_x^2)}{\det(\bar{\Lambda})} = \varepsilon_{yx}, \tag{16}$$

$$\varepsilon_{yy} = \frac{(k+\mathbf{A})^2 + 2(k+\mathbf{A})y\mathbf{A}_y + y^2(\mathbf{A}_x^2 + \mathbf{A}_y^2)}{\det(\bar{\Lambda})}, \tag{17}$$

$$\varepsilon_{zz} = \frac{1}{\det(\bar{\Lambda})}. \tag{18}$$

The relation between the original and transformed coordinates can be established as

$$x = \frac{1}{k}(1 - \mathbf{A}')x', \tag{19}$$

$$y = \frac{1}{k}(1 - \mathbf{A}')y'. \tag{20}$$

Equations (15)–(18) provide full design parameters of the permittivity and permeability tensors for the single conformal cloaking shell $AA'B'B$. The material parameters of other cloaking sections can be obtained in a similar way. Clearly, the cloaks are composed of inhomogeneous and anisotropic metamaterials.

III. FULL-WAVE SIMULATIONS AND DISCUSSIONS

In order to validate the design formulas of the conformal cloak for arbitrary object, we make full-wave simulations on two different heart-shaped cloaks using the commercial software COMSOL MULTIPHYSICS, which is based on the finite-element method. When a transverse-electric- (TE-) polarized plane wave is incident upon a heart-shaped cloak, there exists only the z component of the electric field. Hence this is actually a 2D problem. The computational domain and boundaries are shown in Fig. 3, where perfectly matched layers (PMLs) are employed as the absorbing boundaries. In the following examples of heart-shaped cloaks, the working frequency is 2 GHz and k is set as 0.5. Hence the free-space wavelength is $\lambda = 0.15$ m. The inner boundaries are chosen

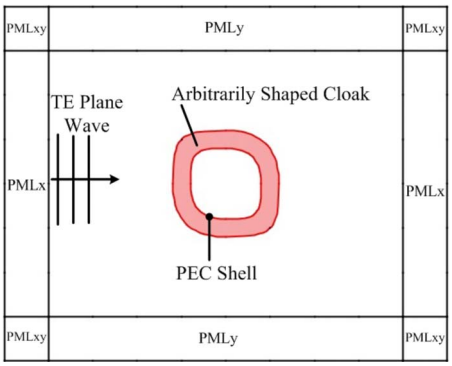

FIG. 3. (Color online) The computational domain and its boundaries used for full-wave simulations of the arbitrarily shaped cloaks. The inner boundary is PEC, and the cloak layer is composed of inhomogeneous and anisotropic materials defined in Eqs. (15)–(18).

to be perfectly electric conductors (PECs) so that no waves can penetrate into the cloaked area. The cloak is composed of the inhomogeneous and anisotropic materials defined in Eqs. (15)–(18).

Figure 4 illustrates the numerical results of electric fields for a heart-shaped cloak and PEC object using different discretizations when the plane waves are incident from the left

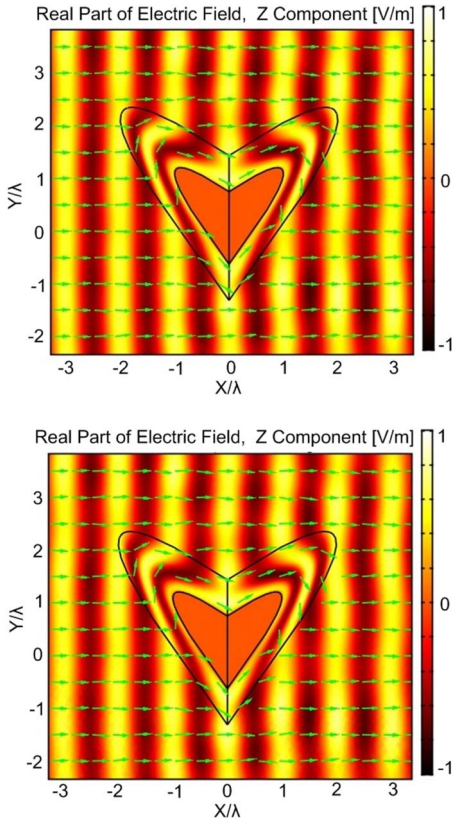

FIG. 4. (Color online) The electric-field distributions and power-flow lines in the computational domain for a heart-shaped cloak and PEC object using different discretizations when the plane waves are incident from the left to the right. (a) 456 000 triangular meshes are used (upper figure). (b) 60 000 triangular meshes are used (lower figure).

to the right. The heart-shaped PEC object (the inner boundary) is divided into two sections: the left and right. The left section is described by the Bézier curve whose control points are $(0,-0.1)$, $(-0.3,0.3)$, and (0, 0.1), respectively. The right section is described by the Bézier curve with the control points $(0,-0.1)$, (0.3, 0.3), and (0, 0.1). In both sections, the control weights are 2, 1, and 2. Hence we can obtain the parametric equations of the two curves as

$$\text{left section:} \quad x(u) = 0.6u^2 - 0.6u, \tag{21}$$

$$y(u) = -0.6u^2 + 0.8u - 0.1, \tag{22}$$

$$\text{right section:} \quad x(u) = -0.6u^2 + 0.6u, \tag{23}$$

$$y(u) = -0.6u^2 + 0.8u - 0.1, \tag{24}$$

in which $u \in [0,1]$. We then can construct the coordinate transformation and compute the permittivity and permeability tensors of the cloak using formulas derived earlier.

When the plane waves are incident from the left to the right, Fig. 4(a) demonstrates the electric-field distributions and the power-flow lines in the computational domain, which is discretized by 456 000 triangular meshes. In the interior region, the fields are zero as predicted; in the cloaking region, we observe that the power-flow lines propagate smoothly around the heart-shaped object and the equal-phase surfaces are warped smoothly in the expected way. Outside the cloak, the TE-polarized plane waves are almost unchanged as if the object does not exist. Hence the invisible cloak for the heart-shaped PEC object is well verified.

In order to study the effect of different discretizations on the invisible properties, we simulate the same heart-shaped cloak and PEC object as that in Fig. 4(a) using 60 000 triangular meshes, which are 7.5 times fewer than those in Fig. 4(a). The simulation results for the electric-field distributions and the power-flow lines are illustrated in Fig. 4(b). Clearly, they are nearly identical to those in Fig. 4(a) even in the concave area of the cloak. We make more simulations using coarser meshes, which show that the permittivity and permeability profiles given by Eqs. (15)–(18) are very stable with discretizations.

Next we consider the invisible properties of the designed cloak in different incident directions. Figure 5 illustrates the electric-field distributions and the power-flow lines in the computational domain when the plane waves are incident from the top and bottom, respectively. In both cases, the power-flow lines with the cloak propagate smoothly around the heart-shaped object, making it invisible. It is even true when the incident waves travel toward the concave area of the cloak, as shown in Fig. 5(a).

In order to observe the reduction of scattering fields at the design frequency with the invisible cloak quantitatively, we have computed the scattered fields of the heart-shaped PEC object on the observation line, $y=0.4$ m, with and without the invisible cloak. Figures 6(a) and 6(b) demonstrate the comparison of such scattered fields when the plane waves are

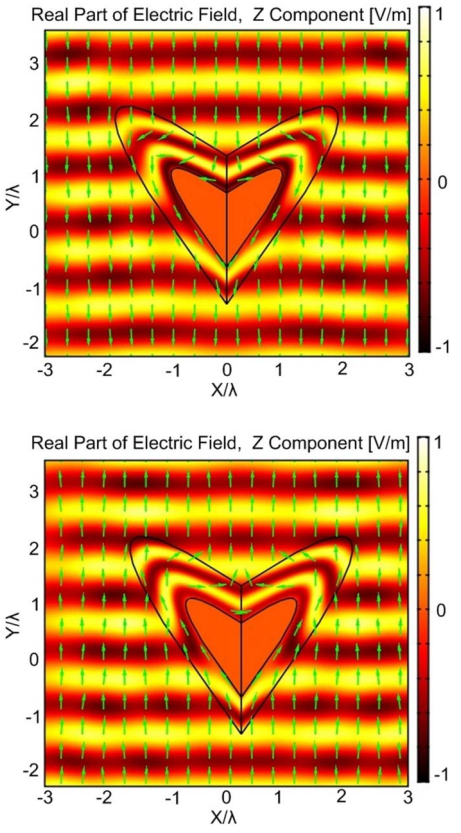

FIG. 5. (Color online) The electric-field distributions and power-flow lines in the computational domain for a heart-shaped cloak and PEC object with different incident directions. (a) The plane waves propagate from the top to the bottom (upper figure). (b) The plane waves propagate from the bottom to the top (lower figure).

incident from the top and bottom, respectively. Figure 6(a) shows a backward-scattering case, and Fig. 6(b) denotes a forward-scattering case. In both cases, the scattered field with the invisible cloak has a significant reduction.

In the above analysis, we have designed a heart-shaped cloak whose boundary is represented by polynomial Bézier curves. Next we give another example of an inverted heart-shaped cloak and PEC object, whose boundary is represented by rational Bézier curves. For the inverted heart-shaped PEC object, we also divide it into two sections. Then the left section is described by the rational Bézier curve with the control points $(0,-0.1)$, $(-0.4,-0.2)$, and (0, 0.1). The right section is described by the rational Bézier curve with the control points $(0,-0.1)$, $(0.4,-0.2)$, and (0, 0.1). In both sections, the control weights are 2, 1, and 2. Hence the parametric equations are obtained as

$$\text{left section:} \quad x(u) = \frac{0.4u^2 - 0.4u}{u^2 - u + 1}, \tag{25}$$

$$y(u) = \frac{0.2u^2 - 0.1}{u^2 - u + 1}, \tag{26}$$

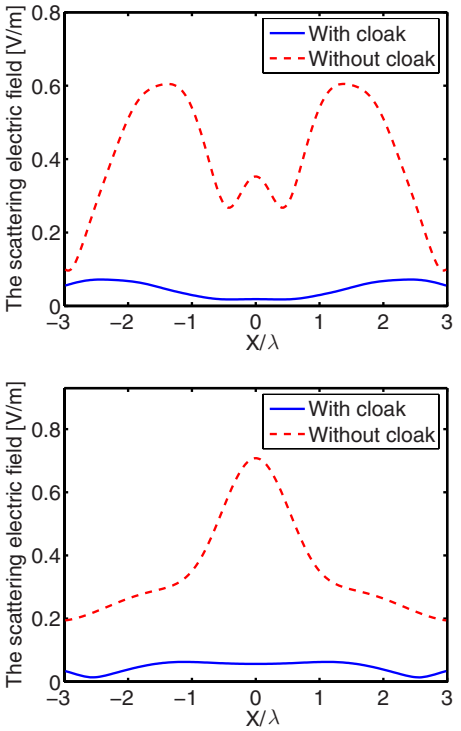

FIG. 6. (Color online) The comparison of scattered electric fields for the heart-shaped PEC object with and without the invisible cloak at the observation line $y=0.4$ m. (a) The incident plane waves propagate from the top to the bottom (upper figure). (b) The plane waves propagate from the bottom to the top (lower figure).

$$\text{right section:} \quad x(u) = \frac{-0.4u^2 + 0.4u}{u^2 - u + 1}, \tag{27}$$

$$y(u) = \frac{0.2u^2 - 0.1}{u^2 - u + 1}. \tag{28}$$

Similar to the earlier example, Fig. 7 illustrates the full-wave simulation results of the inverted heart-shaped PEC object and cloak when the TE-polarized plane waves are incident from the left to the right. As the plane waves pass through the heart cloak, they are guided around the inner PEC object, as shown in Fig. 7(a). Outside the cloak, the plane waves nearly keep their original path and the PEC object is nearly invisible. In order to show the invisible properties clearly, the scattered electric fields from the inverted heart-shaped PEC object with and without the cloak along the observation lines $x=0.4$ m and $x=0.7$ m are computed, as shown in Figs. 7(b) and 7(c), respectively. In Fig. 7(b), the observation line is one wavelength away from the PEC object; in Fig. 7(c), the observation line is three wavelengths away from the PEC object. In both cases, the scattered fields with the invisible cloak are much smaller than those without the cloak. Hence very good effects of the invisibility of the designed cloak have been observed.

IV. CONCLUSIONS

In summary, we have shown how to design conformally invisible cloaks for arbitrary-shaped objects based on the

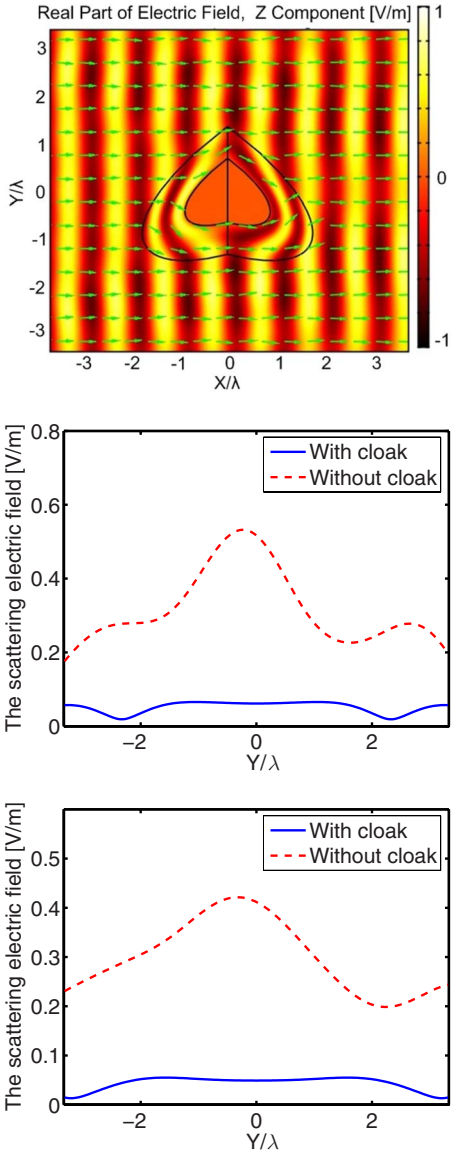

FIG. 7. (Color online) (a) The electric-field distributions and power-flow lines in the computational domain for an inverted heart-shaped cloak and PEC object when the plane waves are incident in the horizontal direction from the left to the right (upper figure). (b) The comparison of scattered electric fields for the inverted heart-shaped PEC object with and without the invisible cloak at the observation line $x=0.4$ m (middle figure). (c) The comparison of scattered electric fields for the inverted heart-shaped PEC object with and without the invisible cloak at the observation line $x=0.7$ m (lower figure).

NURBS curves for geometrical modeling and the corresponding optical transformation method. The proposed approach can also be extended to nonconformal transformations. The application of NURBS in the design of arbitrary cloaks shows the transformation optics to be a very general tool to interface with commercial softwares like 3D STUDIOMAX and MAYA.

In future work, we will investigate simplified formulations of the permittivity and permeability so that the cloaking material can be experimentally realized.

ACKNOWLEDGMENTS

This work was supported in part by the National Basic Research Program (973) of China under Grant No. 2004CB719802, in part by the 111 Project under Grant No. 111-2-05, and in part by the National Science Foundation of China under Grants No. 60671015, No. 60496317, No. 60601002, and No. 60621002.

[1] J. B. Pendry, D. Schurig, and D. R. Smith, Science **312**, 1780 (2006).
[2] U. Leonhardt, Science **312**, 1777 (2006).
[3] D. Schurig, J. J. Mock, B. J. Justice, S. A. Cummer, J. B. Pendry, A. F. Starr, and D. R. Smith, Science **314**, 977 (2006).
[4] D. Schurig, J. B. Pendry, and D. R. Smith, Opt. Express **14**, 9794 (2006).
[5] S. A. Cummer, B.-I. Popa, D. Schurig, D. R. Smith, and J. Pendry, Phys. Rev. E **74**, 036621 (2006).
[6] A. Hendi, J. Henn, and U. Leonhardt, Phys. Rev. Lett. **97**, 073902 (2006).
[7] A. Alu and N. Engheta, Phys. Rev. E **72**, 016623 (2005).
[8] F. Zolla, S. Guenneau, A. Nicolet, and J. B. Pendry, Opt. Lett. **32**, 1069 (2007).
[9] W. Cai, U. K. Chettiar, A. V. Kildishev, V. M. Shalaev, and G. W. Milton, Appl. Phys. Lett. **91**, 111105 (2007).
[10] H. Chen and C. T. Chan, Appl. Phys. Lett. **90**, 241105 (2007).
[11] Y. Huang, Y. Feng, and T. Jiang, Opt. Express **15**, 11133 (2007).
[12] B. Zhang, H. Chen, B.-I. Wu, Y. Luo, L. Ran, and J. A. Kong, Phys. Rev. B **76**, 121101(R) (2007).
[13] W. Cai, U. K. Chettiar, A. V. Kildishev, and V. M. Shalaev, Nat. Photonics **1**, 224 (2007).
[14] H. Chen, B. I. Wu, B. Zhang, and J. A. Kong, Phys. Rev. Lett. **99**, 063903 (2007).
[15] Z. Ruan, M. Yan, C. W. Neff, and M. Qiu, Phys. Rev. Lett. **99**, 113903 (2007).
[16] H. Chen and C. T. Chan, Appl. Phys. Lett. **90**, 241105 (2007).
[17] M. Rahm, S. A. Cummer, D. Schurig, J. B. Pendry, and D. R. Smith, Phys. Rev. Lett. **100**, 063903 (2008).
[18] W. X. Jiang, T. J. Cui, Q. Cheng, J. Y. Chin, X. M. Yang, R. Liu, and D. R. Smith, Appl. Phys. Lett. (to be published).
[19] A. Greenleaf, Y. Kurylev, M. Lassas, and G. Uhlmann, Commun. Math. Phys. **275**, 749 (2007).
[20] F. L. Teixeira, IEEE Antennas Wirel. Propag. Lett. **6**, 163 (2007).
[21] M. Rahm, D. Schurig, D. A. Roberts, S. A. Cummer, D. R. Smith, and J. B. Pendry, Photonics Nanostruct. Fundam. Appl. **6**, 87 (2008).
[22] L. Piegl and W. Tiller, *The NURBS Book*, 2nd ed. (Springer-Verlag, New York, 1996).